

Supplementary Information for

**Bio-inspired Self-Breathable Structure Driven by Volumetric
Effect: An Unusual Driving Force of Metal Sulfide for High
Alkaline Ions Storage Capability**

Qujiang Sun ^{a, b}, HongLiang Wu ^d, Hai Ming ^e, Lianshan Sun ^a, Lin Zhou ^{a, b}, Chunli
Wang ^{a, c}, Xuxu Wang ^{a, c}, Limin Wang ^{a*}, Jun Ming ^{a*}

^a *State Key Laboratory of Rare Earth Resource Utilization, Changchun Institute of Applied Chemistry, CAS, Changchun, 130022, P. R. China.*

^b *University of Chinese Academy of Sciences, Beijing, 100049, P. R. China.*

^c *University of Science and Technology of China, Hefei, P. R. China.*

^d *Shuangdeng Group Co.,Ltd., Jiangyan 225526, P. R. China.*

^e *Research Institute of Chemical Defense, Beijing 100191, P. R. China.*

E-mail: lmwang@ciac.ac.cn (L. Wang); jun.ming@ciac.ac.cn (J. Ming).

Experimental

Materials. The spores of *Lycoperdon Bovista* (SLBs) were collected in nature. The chemicals of ethanol (A.R., >99.7%), sodium molybdate (Na_2MoO_4 , A.R., >99.5%) and thiourea (Tu, A.R., >99.5%) were purchased from Beijing Chemical Reagent Co. Ltd. All reagents were used without further purification.

Synthetic Procedures. The collected SLBs was washed by ethanol and deionized water (DIW) several times to remove the impurities, and then vacuum freeze-dried. The dried SLBs were carbonized to N-C in tube furnace at 1000 °C for 5 h under the Ar/H₂ (9/1, v/v) flow, where the ramping speed is controlled at 5 °C min⁻¹. Later, 50 mg N-C was dispersed first in 60 mL DIW under ultrasonic dispersion for 30 min, and then 0.12 g Na₂MoO₄ and 0.24 g thiourea were dissolved into the solution. After 1 h ultrasonic treatment, the black solution was transferred to a 100 mL Teflon-lined stainless-steel autoclave and hydrothermal-treated at 200 °C for 24 h. The intermediates were filtered, washed with DIW, and then freeze-dried. Finally, the N-C@MoS₂ was obtained through the calcination at 700 °C for 2 h under the Ar/H₂ flow, where the heating rate is controlled at 2 °C min⁻¹.

The similar synthetic procedure is extended to the N-C@SnS. Typically, 50 mg N-C was dispersed first in 60 mL DIW under ultrasonic treatment for 30 min, and then 0.168 g SnCl₄ and 0.228 g thiourea were added and dissolved. After 1 h ultrasonic treatment, the black solution was transferred to a 100 mL Teflon-lined stainless-steel autoclave and hydrothermal-treated at 180 °C for 12 h. The intermediates were filtered, washed with DIW, and then freeze-dried. Finally, the

N-C@SnS was obtained through the calcination at 500 °C for 1 h under the Ar/H₂ flow, where the heating rate is controlled at 2 °C min⁻¹.

Materials Characterization. The crystalline information was acquired by X-ray diffractometer (XRD, Bruker D8 Focus) at a scan speed of 2° min⁻¹ with copper K α radiation. The morphology was characterized by scanning electron microscope images (SEM) operating on field emission Hitachi S-4800 instrument at the accelerating voltage of 10 kV. The structural information and element mapping were observed by transmission electron microscopy (TEM) and high-angle annular dark-field scanning transmission electron microscopy (HAADF-STEM) on FEI Tecnai G2 S-Twin instrument with field emission gun operating at 200 kV. The carbon content in composite was analyzed by thermogravimetric (TG) analysis within the temperature of 25-800 °C with the heating rate of 10 °C min⁻¹ under air flow using the STA 449 Jupiter (NETZSCH) thermogravimetry analyser. The BET surface area and porosity were determined by N₂ adsorption/desorption measurements conducted with Micromeritics ASAP 2010 instrument at -196 °C after the sample was degassed at 200 °C for 6 h under vacuum conditions. The pore size distribution curves were estimated from the adsorption isotherms using the Barrett–Joyner–Halenda (BJH) method.

Electrochemical measurements. The electrode was prepared as below. The active material of N-C@MoS₂, carbon black and Polyacrylic acid (PAA) with the mass ratio of 7:2:1 were mixed in DIW to form a uniform slurry and then casted on copper foil. The electrode was vacuum-dried at 80 °C overnight, where the areal mass density of

N-C@MoS₂ was controlled at 1.5 mg cm⁻². The electrochemical measurements were performed using the CR 2032-type coin cell, which has the configuration of working electrode | Celgard 2400 membrane separator (or glass microfiber) | metallic lithium (or sodium foil). The electrolyte of 1.0M LiPF₆ in ethyl carbonate (EC)/diethyl carbonate (DEC) (1:1, v/v) or 1 M NaClO₄ in a mixture of EC/dimethyl carbonate (DMC) (1:1, v/v) was used for the lithium and sodium battery, respectively. The cell was assembled in glovebox, in which the moisture and oxygen were strictly controlled below 0.1 ppm. Galvanostatic charge-discharge performances were measured under the cut-off voltage of 0.01-3.0 V using the Land battery testing system at room temperature. Cyclic voltammetry (CV) measurement was conducted on BioLogic VMP3 electrochemical workstation at the scan rate of 0.1 mV s⁻¹. In addition, the electrochemical impedance spectroscopy (EIS) was carried out within the range of 10 mHz-100 kHz with an applied amplitude of 5 mV.

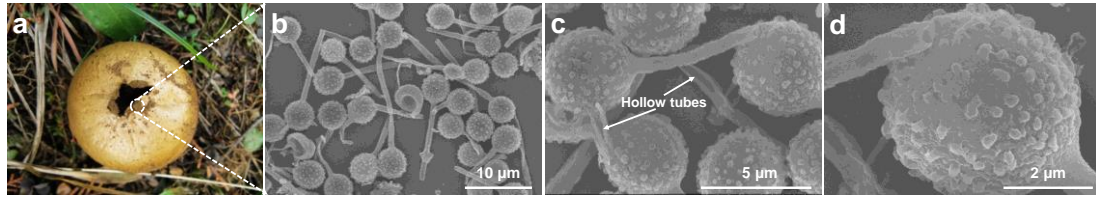


Figure S1. Characterizations of spores of *Lycoperdon Bovista* (SLBs). (a) Typical digital photograph of raw *Lycoperdon Bovista*. (b-d) FESEM images of raw SLBs with different magnifications.

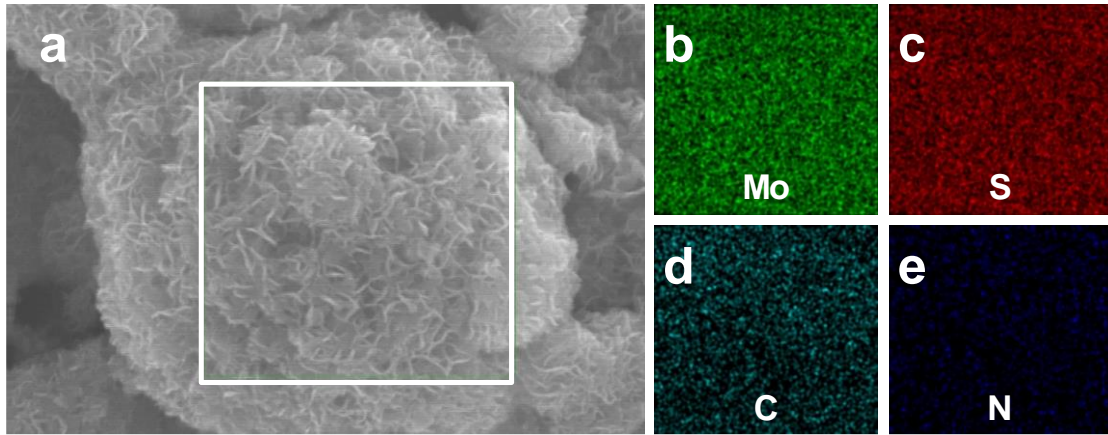


Figure S2. Elemental mapping of N-C@MoS₂. (a) SEM image. Mapping images of (b) Mo, (c) S, (d) C and (e) N.

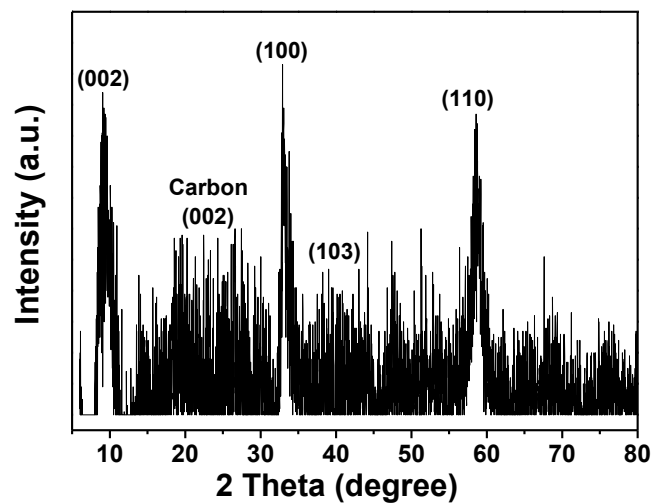


Figure S3. Characterizations of N-C@MoS₂. (a) XRD patterns of N-C@MoS₂ after deducting the background.

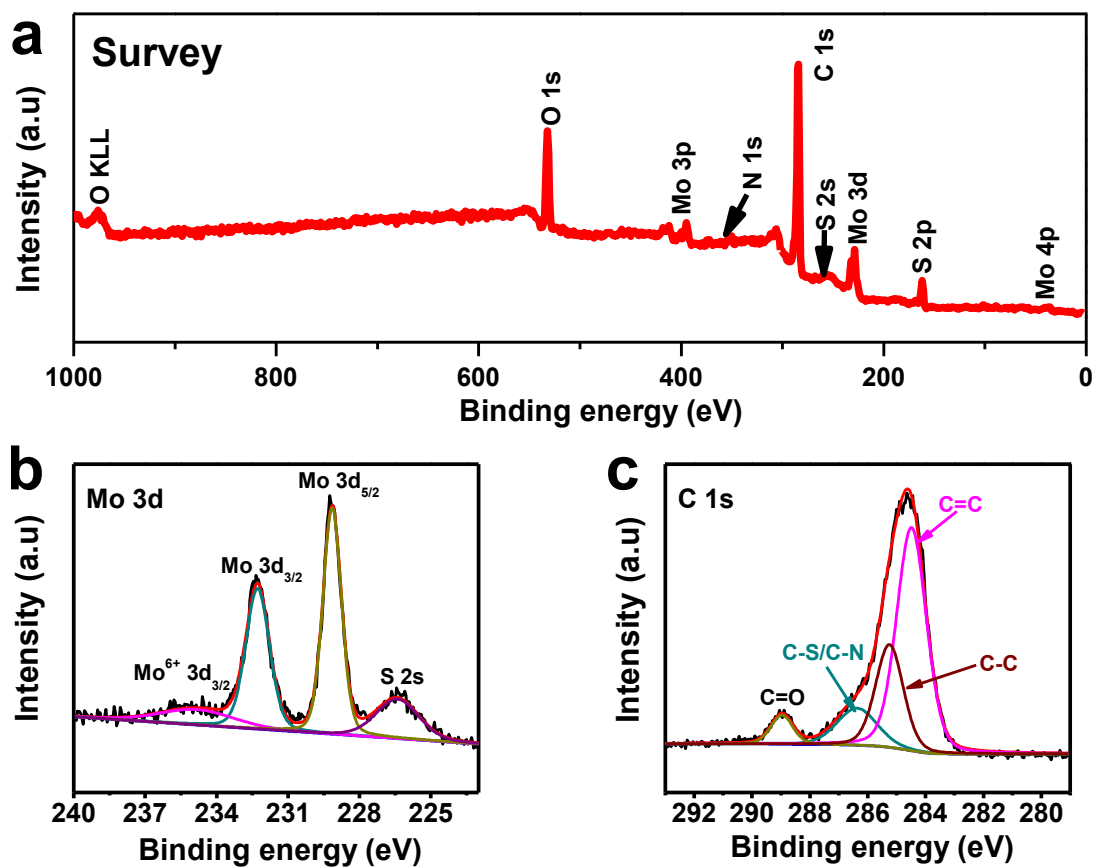


Figure S4. Characterizations of N-C@MoS₂. (a) Survey X-ray photoelectron spectroscopy (XPS) spectrum of the N-C@MoS₂. High-resolution spectra of (b) Mo 3d and (c) C 1s.

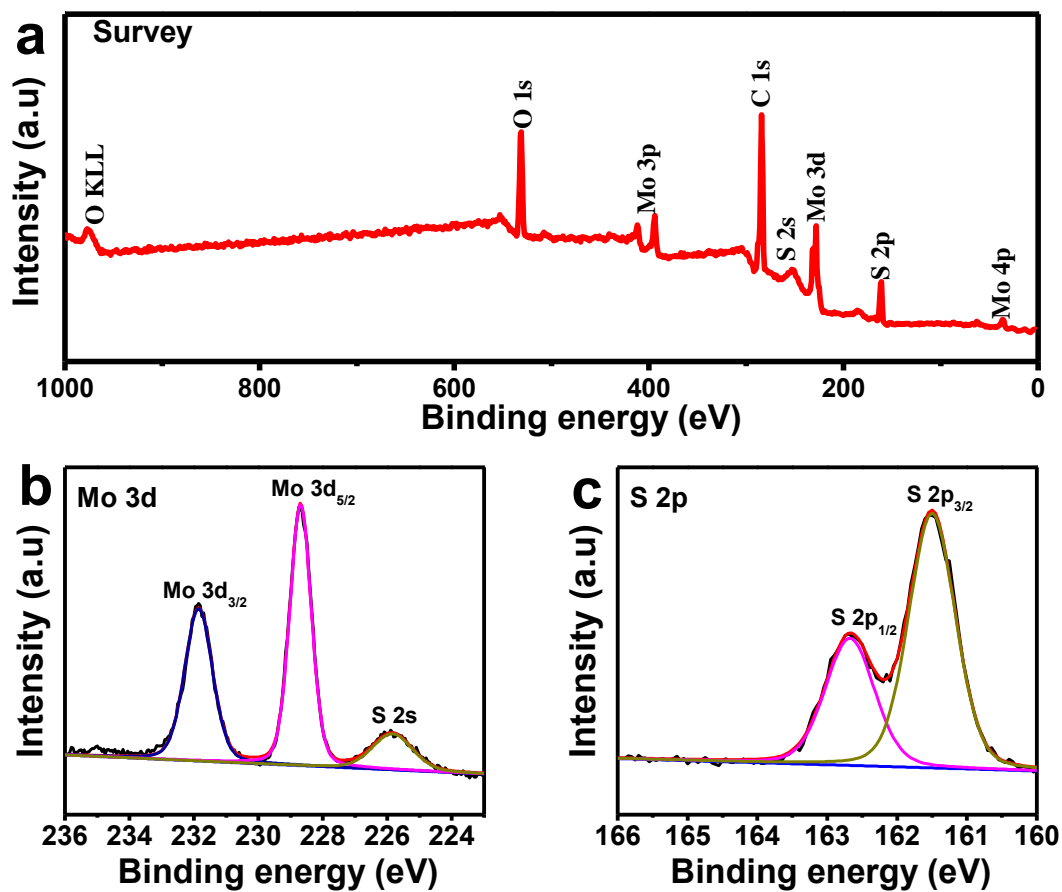


Figure S5. Characterizations of bare MoS₂. (a) Survey X-ray photoelectron spectroscopy (XPS) spectrum of bare MoS₂. High-resolution spectra of (b) Mo 3d and (c) C 1s.

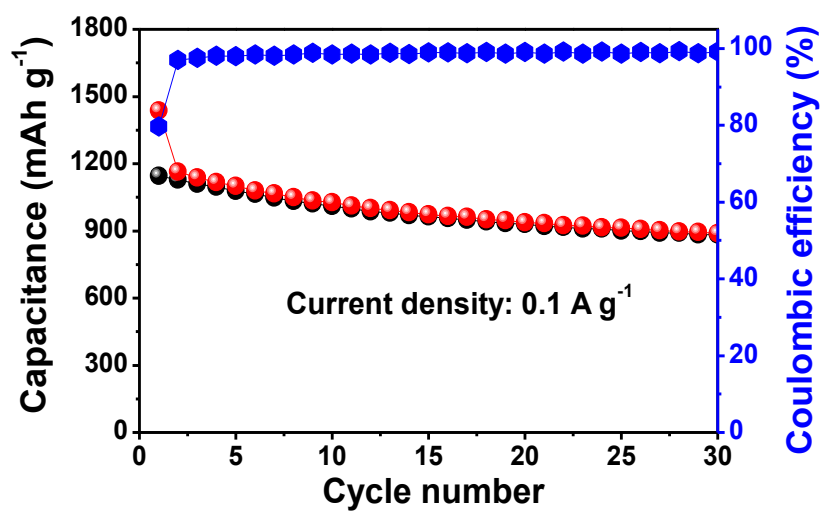


Figure S6. Lithium storage capability of N-C@MoS₂. Cycle performance of N-C@MoS₂ at the current density of 0.1 A g⁻¹.

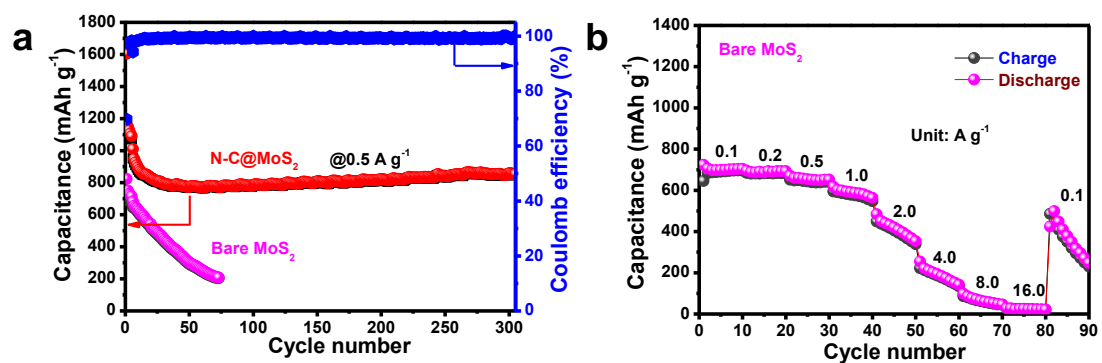


Figure S7. Lithium storage performance of N-C@MoS₂ and bare MoS₂. (a) Comparative cycle performances at the current density of 0.5 A g⁻¹. (b) Rate capability of the bare MoS₂.

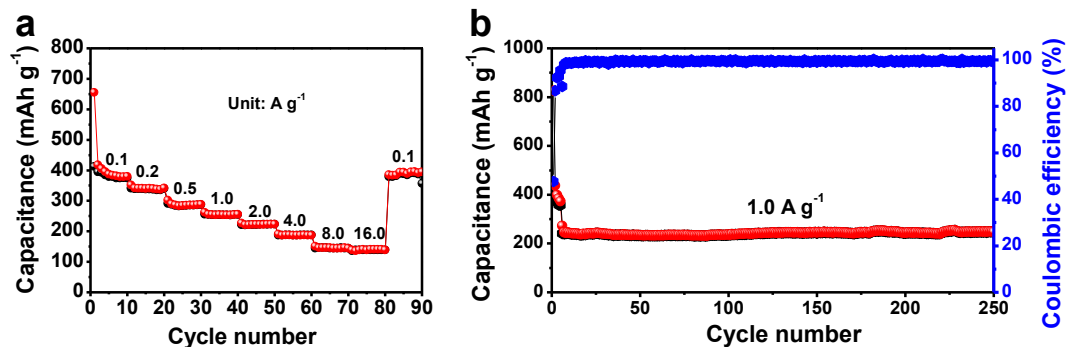


Figure S8 Lithium storage capability of N-C. (a) Rate capabilities at the current density of 0.1-16.0 A g⁻¹ and (b) cycling performance at the current density of 1.0 A g⁻¹. The capacities of N-C can achieve as high as 390, 288, 223, 146, and 139 mAh g⁻¹ at the current density of 0.1, 0.5, 2, 8, and 16 A g⁻¹, respectively. In addition, the electrode can cycle more than 250 cycles with an average capacity of 242 mAh g⁻¹ at the current density of 1 A g⁻¹ even after the rate test.

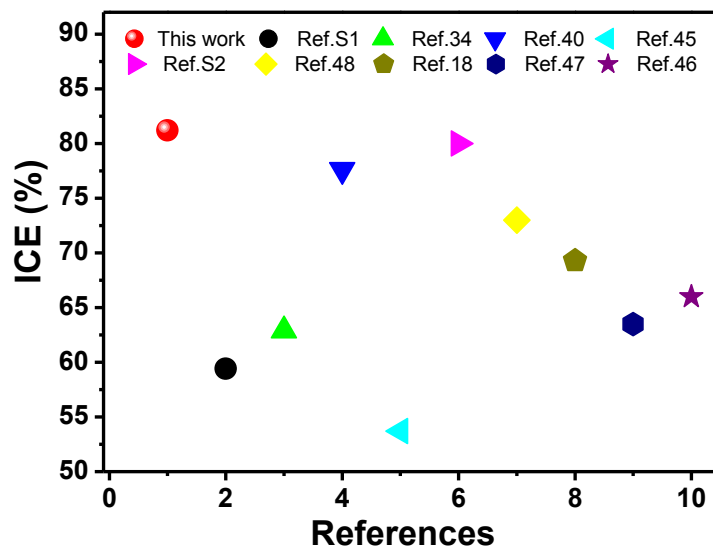


Figure S9. Comparative ICE of the N-C@MoS₂ and the MoS₂-based anode reported before.

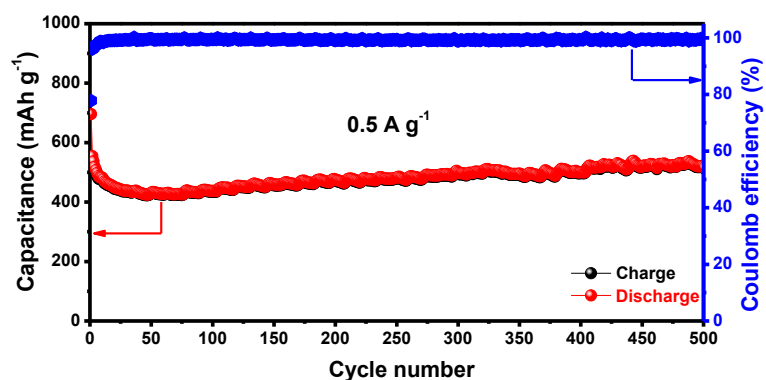


Figure S10. Lithium storage capacity of N-C@MoS₂ with a high loading of 3.2 mg cm⁻². Note that the mass loading of N-C@MoS₂ anode around at 1.5 mg cm⁻² should be appropriate. This is because the specific capacity of anode is much higher than that of cathode. For example, the calculated mass loading of cathode (e.g., lithium layered oxide, LiCoO₂, 150 mAh g⁻¹) should be around 10 mg cm⁻² when the cathode match with the anode, because the total capacity of N-C@MoS₂ anode can achieve as high as 1500 mAh cm⁻² (i.e., 1.5 mg cm⁻² * 1000 mAh g⁻¹ = 1500 mAh cm⁻²/150 mAh g⁻¹ = 10 mg cm⁻² cathode).

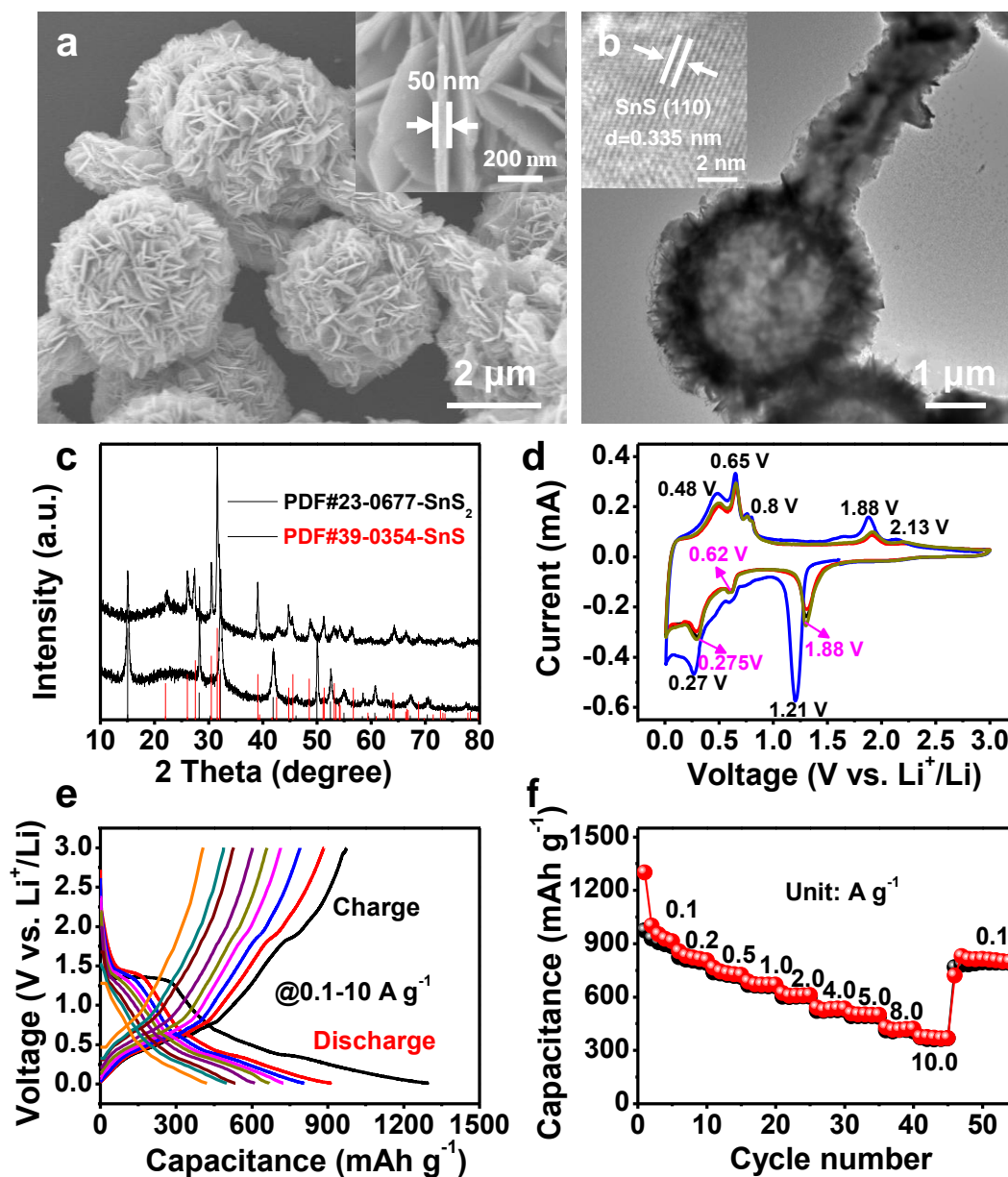


Figure S11. Characterizations and electrochemical performance of N-C@SnS. (a) FESEM and (b) (HR-) TEM images of N-C@SnS. (c) XRD patterns of N-C@SnS. (d) cyclic voltammetry and (e) Voltage vs. capacity profile of N-C@SnS at the current density of 0.1-10 A g⁻¹. (f) Rate capabilities of N-C@SnS electrode.

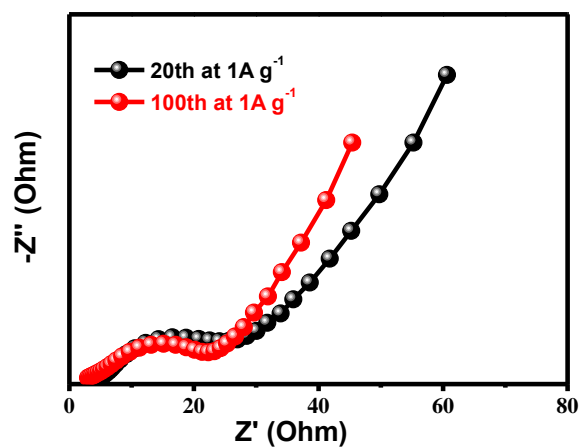


Figure S12. Electrochemical analysis. The electrochemical impedance spectra (EIS) of cycled N-C@MoS₂ electrodes for LIBs at the current density of 1.0 A g⁻¹.

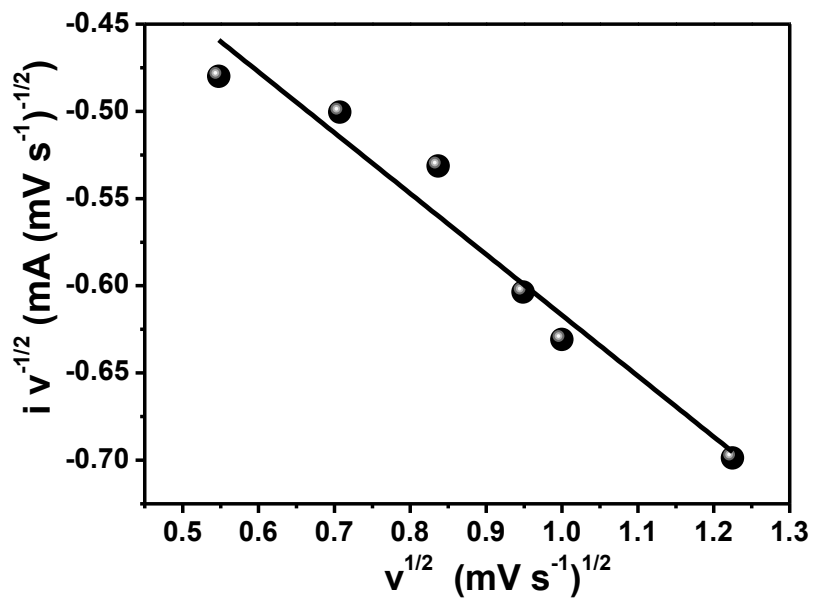


Figure S13. Linear behavior of $i(V) / v^{1/2}$ as a function of $v^{1/2}$. This is used to determine the slope (k_1) and intercept (k_2) of the equation ($i = k_1 v + k_2 v^{1/2}$).

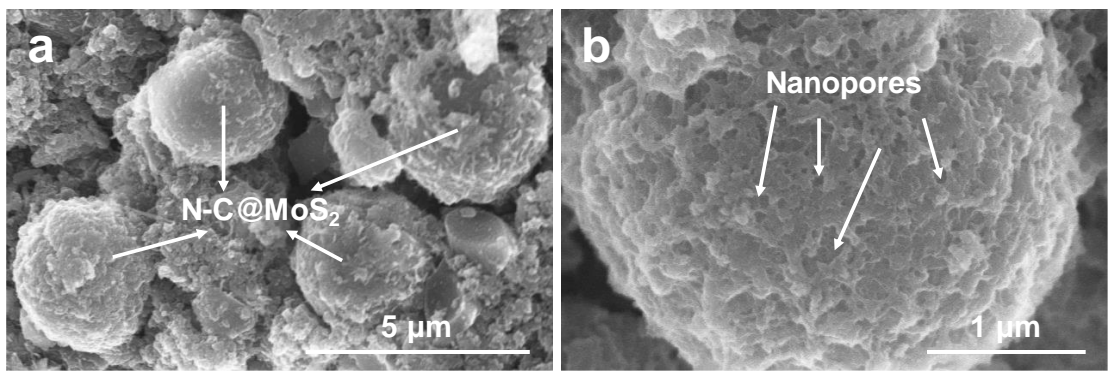


Figure S14. Characterization of cycled N-C@MoS₂. The morphology of N-C@MoS₂ is well stabilized when the electrode was cycled at 1.0 A g⁻¹ for 50 cycles, demonstrating the good structural stability of N-C@MoS₂ upon (de-)lithiation process.

Table S1 Comparative performance of N-C@MoS₂ and MoS₂-based anode reported before at a low current density.

MoS ₂ -based materials	Synthetic Method	Loading density (mg cm ⁻²)	Current density (A g ⁻¹)	Capacity (mAh g ⁻¹)	Ref.
PCNFs@MoS ₂	Electrospinning-solvothermal	--	0.05	736	45
G/TiO ₂ @C/MoS ₂ composite	Hydrothermal treatment	0.8	0.1	802	40
MoS ₂ -RGO composite	Hydrothermal treatment	0.8-1	0.1	860	41
TiO ₂ /MoS ₂ hybrids	Exfoliation method	1.0	0.1	623	48
E-MoS ₂ @NC	Exfoliation method	--	0.2	800	49
MoS ₂ -cBC	Hydrothermal treatment	--	0.1	864	46
NDG/MoS ₂ /NDG	Thermal decomposition reduction method	1.0	0.1	750	31
TiO ₂ @NC@MoS ₂	Template method	--	0.1	925	S1
C@MoS ₂ @C hollow spheres	Template method	1.0	0.067	857	47
MoS ₂ /C aerogel	Sol-gel method	--	0.1	653	34
Aurilave-like N-C@MoS ₂	Bio-template method	1.5	0.1	966	This work

Table S2 Impedance parameters, R_s , R_{SEI} and R_{ct} , obtained from the EIS plots in **Figure 6a**.

Sample	R_s (Ω)	R_{SEI} (Ω)	R_{ct} (Ω)
Bare MoS ₂	2.57	16.11	105.65
N-C@MoS ₂	2.42	11.51	55.65

REFERENCES

- S1 S. Wang, B. Y. Guan, L. Yu and X. W. D. Lou, *Adv. Mater.* **2017**, 29, 1702724-1702729.
- S2 Y. F. Chao, R. Jalili, Y. Ge, C. Y. Wang, T. Zheng, K. W. Shu, and G. G. Wallace, *Adv. Funct. Mater.* **2017**, 27, 1700234-1700244.